17th World Conference on Earthquake Engineering, 17WCEE
Sendai, Japan - September 13th to 18th 2020

SHAKING TABLE TEST AND REAL-TIME HYBRID SIMULATION IN SEMI-ACTIVE CONTROLLED BASE-ISOLATION SYSTEM

K. Itahara[(1)], H. Fujitani[(2)], Y. Mukai[(3)], M. Ito[(4)], E. Sato[(5)], S. Iba[(6)]

[(1)] *Graduate student, Graduate School of Engineering, Kobe University, 185t005t@kobe-u.ac.jp*
[(2)] *Professor, Graduate School of Engineering, Kobe University, fujitani@kobe-u.ac.jp*
[(3)] *Associate Professor, Graduate School of Engineering, Kobe University, ymukai@port.kobe-u.ac.jp*
[(4)] *Senior Research Engineer, Building Research Institute, mai_ito@kenken.go.jp*
[(5)] *Senior Researcher, National Research Institute of Earth Science and Disaster Resilience, eiji@bosai.go.jp*
[(6)] *Graduate student, Graduate School of Engineering, Kobe University, 180t008t@kobe-u.ac.jp*

Abstract

A base-isolation system requires large base-isolation clearance in the event of a large earthquake. If numerous passive dampers are installed in a base-isolation system to reduce the base-isolation response displacement, then the response acceleration increases. Consequently, the base-isolation system characteristics are impaired. For this study, semi-active control is performed by installing an MR damper, a variable damper, in the base-isolation system with the goal of reducing the response displacement without increasing response acceleration. Results confirmed the response reduction effect. As a verification method, a shaking table test and real-time hybrid simulation (RTHS) were applied. The RTHS effectiveness was verified by comparing shaking table test results obtained using a large-scale base-isolated building model at E-Defense and RTHS results obtained using the shaking table at Kobe University. Using RTHS, one can perform tests with mutual interaction in real time. The part for which the characteristic is not well understood is actually tested. Moreover, the part for which the characteristic is well understood is subjected to computer analysis. In this study, RTHS method uses computer analysis of the base-isolation system. Only a magnetorheological (MR) damper is installed between the shaking table and the reaction wall. The base-isolation layer displacement obtained through the computer analysis is reproduced on the shaking table. The obtained damper force controls the base-isolation system in the computer analysis. Furthermore, RTHS allows the target building to be changed freely. Various base-isolation systems were tested to verify the effectiveness of semi-active control. For this study, linear quadratic regulator (LQR) control, a state feedback control method, was used as a semi-active control law. Furthermore, response reduction effects were anticipated by application of control combining feedback control with feedforward control.

Keywords: *Base-isolation system, MR damper, Real-time hybrid simulation, Semi-active control, Shake table test*

Photo 1 – Schematic view of E-Defense test

Photo 2 – Schematic view of real-time hybrid simulation

1. Introduction

The occurrence of an earthquake beyond the assumed earthquake scale leads to damage such as deformation of the base-isolated layer exceeding the base isolation clearance and collision with the retaining wall. Therefore, sufficient base isolation clearance must be secured. Nevertheless, securing sufficient base isolation clearance is difficult in an urban area where buildings are densely packed. Therefore, it is important to reduce the response displacement of the base-isolation layer. However, if the response displacement is reduced by increasing the number of conventional passive dampers, then acceleration of the upper structure will increase and the isolation structure characteristics will be impaired. This study was conducted to reduce the base-isolation layer displacement and avoid increasing the building acceleration by application of semi-active control using a magnetorheological (MR) damper for a base isolation structure. Various semi-active control rules have been proposed. Their effectiveness has been demonstrated. For this study using linear quadratic regulator (LQR) control, its effectiveness is confirmed using the MR damper attached to the base-isolation layer.
The semi-active control effectiveness will be verified by shaking table tests using the large base isolation specimen at E-defense, using real-time hybrid simulation (RTHS) at Kobe University, and through analysis. Actually, RTHS is an experimental method by which simultaneous interaction in real time for analysis is reproduced by modeling and experimentation, and sometimes using real objects for those which are difficult to reproduce. When evaluating the response of a structure during an earthquake, a vibration test using a shaking table is often applied to measure the behavior. However, as the structure size increases, greater costs and time requirements become burdensome. Certainly, a capacity limit of shaking tables exists. Therefore, Saeki proposed [1] an experimental method using real objects for vibration experiments to evaluate the response at the time of an earthquake. Other evaluation can be done by combining response calculations with computer analysis.
By applying RTHS, one can confirm the overall response that incorporates the inaccurate modeling. Subsequently, the effectiveness of RTHS is confirmed by comparing shaking table test results using a large base isolation specimen at E-defense, RTHS at Kobe University, and additional analysis.

2. Experiment Outline

2.1 MR Damper

2.1.1 Modeling of the MR Damper

When no magnetic field acts on the MR fluid, the shear stress increases in proportion to the velocity. When a magnetic field acts on the MR fluid, it has yield stress according to the magnetic field strength. Thereafter the shear stress increases in proportion to the velocity. The damper force can be varied by changing the magnetic field strength. The MR damper was tested with the sinusoidal excitation experiment under various conditions. A Bingham plastic model (Fig. 2) is shown as a mechanical model of the MR damper. The damper force F_{MR} of the MR damper was modeled as Eq. (1) based on the sinusoidal excitation experiment (Fig. 3) (Table 1). Good correspondence is apparent from comparison of the Bingham plastic model with the sinusoidal excitation experiment. However, the model has low reproducibility in a low-speed region.

$$F_{MR} = (-0.226I^2 + 2.867I - 0.203) * sign(v) + 2.11v \quad (1)$$

(F_{MR}(kN), v(m/s), I(A))

2.1.2 Frequency characteristic of the MR Damper

The damper force of the MR damper does not switch immediately with a change in current. To confirm the followability of the damper force to a current at a certain frequency, the MR damper is applied as a triangular wave. A current is applied as sinusoidal (Table 2) [2]. Fig. 4 shows the MR damper frequency characteristics.

Fig. 1 – MR damper

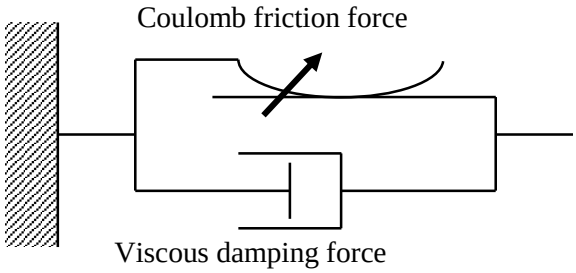

Fig. 2 – Bingham Plastic model

Table 1 – Sinusoidal excitation experiment

Amplitude	Frequency
±200 mm	0.2 Hz, 0.33 Hz, 0.5 Hz
±100 mm	0.2 Hz, 0.33 Hz, 0.5 Hz, 1 Hz

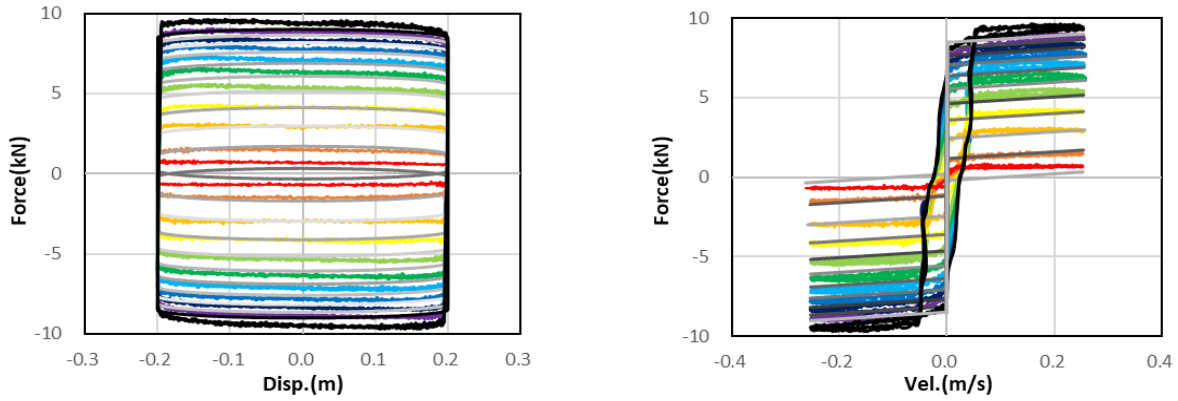

Fig. 3 – Sinusoidal excitation experiment (±200 mm amplitude, 0.2 Hz frequency)

It can be confirmed that the performance drops from about 8 Hz. The damping force of the MR damper is assumed to be divisible into a Coulomb friction force and a viscous damping force. The current is considered to affect only a Coulomb friction force. Eq. (2) represents the transfer function between a current and a Coulomb friction force (Fig. 4).

$$H_{(s)} = \frac{(2\pi\times19.35)\times1.7}{(s+2\pi\times19.35)} \tag{2}$$

The damper force of the MR damper is simulated by adding the inverse Laplace transform of the transfer function $H_{(s)}$ and a viscous damping force (Eq. (3)). Then this model is set as a frequency model.

$$F_{MR} = \mathcal{L}^{-1}\left(\frac{(2\pi\times19.35)\times1.7}{(s+2\pi\times19.35)} \times I_{(s)}\right) + 2.11 \times v \tag{3}$$

Table 2 – Triangular wave excitation

MR damper		Current	
Amplitude	Frequency	Amplitude	Frequency
±250 mm	0.1 Hz	0.5–4.5A	0.5 Hz, 1 Hz, 2 Hz, 4 Hz, 6 Hz, 8 Hz, 10 Hz, 15 Hz, 20 Hz, 25 Hz, 30 Hz

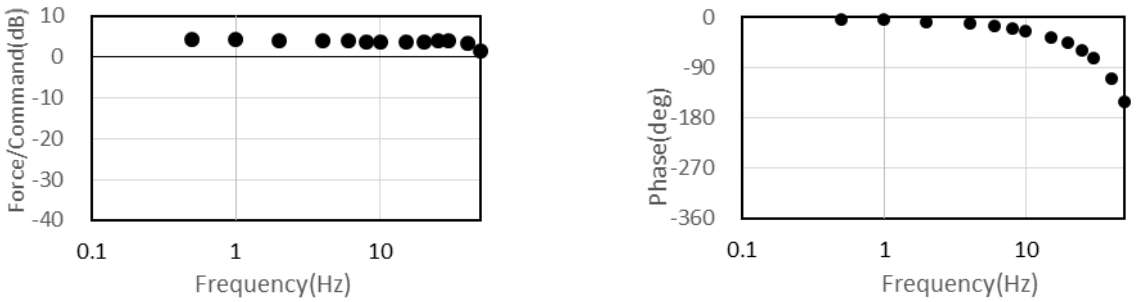

Fig. 4 – Frequency characteristics of current and Coulomb friction force of an MR damper

2.2 Large Base Isolation Specimen

Fig. 5 presents an overview of the base isolation specimen. The specimen is placed at the center of the shaking table. Then the specimen is vibrated in the X-axis direction. The direction of the upper structure is restricted using a linear slider. The MR damper is mounted in the X-axis direction. The specimen mass was measured using a load cell and was found to be 14.863 ton. As shown in Fig. 5, the superstructure can have two mass points. However, the superstructure stiffness is regarded as much higher than that of the base-isolation layer. It can therefore be regarded as one mass point.

Fig. 5 – Overview of the base isolation specimen

The stiffness and damping constant of the laminated rubber were ascertained from the results of single vibration. Fig. 6 shows the displacement-load hysteresis of the laminated rubber. Therefore, the stiffness was set to 42.3 (kN/m). The damping constant was set to 3.58 (%). Furthermore, the frictional force (F_f) by the linear slider was expressed by Eq. (4), with F = 2 kN and α = 200. This value was determined from a parameter study.

$$F_f = F \tanh \alpha v \tag{4}$$

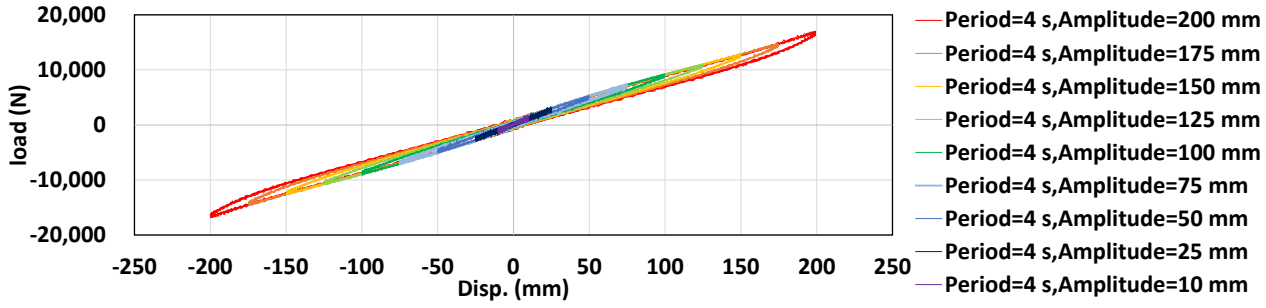

Fig. 6 Displacement–load hysteresis of the laminated rubber

2.3 Real-Time Hybrid Simulation

Fig. 7 presents an outline of RTHS of MR damper alone. In RTHS, a ground motion is input to the base isolation specimen in a computer. Then the time history response analysis is performed. The response base-isolation layer displacement is reproduced on the shaking table. The load measured by the load cell attached to the MR damper is fed back to the specimen in the computer. The response of the next step of the specimen subjected to the load measured by the load cell is returned. Then, calculation of the semi-active control is performed using the response value of the specimen in the computer to ascertain the damper force. This operation is then repeated at 500 Hz intervals.

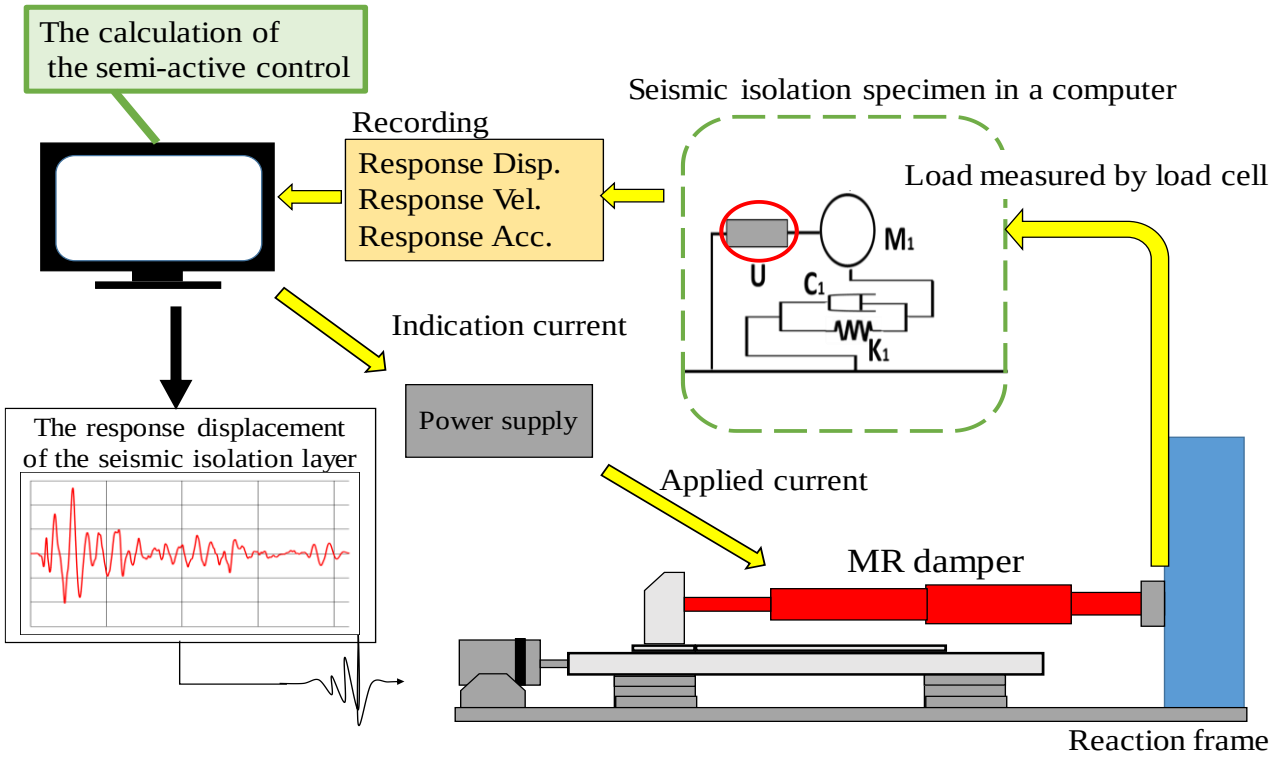

Fig. 7 – Outline of RTHS of MR damper alone

3. Semi-active control strategy

3.1 LQR considering ground motion [3]

We can anticipate further control effects by considering the influences of ground motion, an external disturbance, on optimal control, which is feedback control. Assuming the input disturbance velocity ($\dot{x}_g$) as white noise and modeling the system with a low-pass filter (Eq. (5)), control can be performed actively in the frequency band including the resonance frequency affecting the building control.

$$H_g = \frac{\dot{Z}_{(s)}}{w_{(s)}} = \frac{(2\pi f_g)^2}{s^2+2h_g(2\pi f_g)s+(2\pi f_g)^2} \tag{5}$$

Convert transfer function (Eq. (5)) to a differential equation (Eq. (6) and Eq. (7)).

$$\dot{\boldsymbol{z}} = \boldsymbol{A_z z} + \boldsymbol{B_z} w \tag{6}$$

$$\ddot{\boldsymbol{x}}_{\boldsymbol{g}} = \boldsymbol{C_z z} \tag{7}$$

$$\boldsymbol{A_z} = \begin{bmatrix} 0 & 1 \\ -(2\pi f_g)^2 & -2h_g 2\pi f_g \end{bmatrix}, \boldsymbol{B_z} = \begin{bmatrix} 0 \\ (2\pi f_g)^2 \end{bmatrix}, \boldsymbol{C_z} = \begin{bmatrix} 0 \\ 1 \end{bmatrix}, \mathbf{z} = \begin{bmatrix} \dot{x}_g \\ \ddot{x}_g \end{bmatrix}, f_g\text{: cutoff frequency}$$

The model which combines models of both the specimen and the round motion is represented as one overall model. Eq. (8) and Eq. (9) show the state equation when the target building is a one-mass system.

$$\dot{\boldsymbol{X}}' = \boldsymbol{A}'\boldsymbol{X}' + \boldsymbol{B}'u + \boldsymbol{E}'w \tag{8}$$

$$\boldsymbol{A}' = \begin{bmatrix} 0 & 1 & 0 & 0 \\ -\frac{k}{m} & -\frac{c}{m} & 0 & -1 \\ 0 & 0 & 0 & 1 \\ 0 & 0 & -(2\pi f_g)^2 & -2h_a 2\pi f_g \end{bmatrix},\ \boldsymbol{X}' = \begin{Bmatrix} x \\ \dot{x} \\ \dot{x_g} \\ \ddot{x_g} \end{Bmatrix},\ \boldsymbol{B}' = \begin{Bmatrix} 0 \\ -\frac{1}{m} \\ 0 \\ 0 \end{Bmatrix},\ \boldsymbol{E}' = \begin{Bmatrix} 0 \\ 0 \\ 0 \\ 0 \\ (2\pi f_g)^2 \end{Bmatrix},$$

$$\mathbf{Y} = \boldsymbol{C}'\boldsymbol{X}' + \boldsymbol{D}'u \tag{9}$$

$$\mathbf{Y} = \begin{Bmatrix} x \\ \dot{x} \\ \ddot{x} + \ddot{z} \end{Bmatrix}, \qquad \boldsymbol{C}' = \begin{bmatrix} 1 & 0 & 0 & 0 \\ 0 & 1 & 0 & 0 \\ -\frac{k}{m} & -\frac{c}{m} & 0 & 0 \end{bmatrix}, \boldsymbol{D}' = \begin{Bmatrix} 0 \\ 0 \\ -\frac{1}{m} \end{Bmatrix}$$

x, structure displacement; *m*, mass; *k*, stiffness; *c*, damping coefficient; *z*, ground motion displacement

Each gain is found using the evaluation function of Eq. (10). The MR damper exerts the optimum control force.

$$J = \frac{1}{2}\int (\boldsymbol{Y}^T\boldsymbol{Q}\boldsymbol{Y} + ru^2)dt \tag{10}$$

$$\boldsymbol{Q} = \begin{bmatrix} \alpha_d & 0 & 0 \\ 0 & \alpha_v & 0 \\ 0 & 0 & \alpha_a \end{bmatrix}, \alpha_d \cdot \alpha_v \cdot \alpha_a \cdot u : \text{Weight coefficient}$$

3.2 LQR considering restoring force [4]

Eq. (11) represents the equation of motion of the absolute coordinate system of a one mass system.

$$m(\ddot{x} + \ddot{z}) + c(\dot{x} + \dot{z}) + k(x + z) = c\dot{z} + kz \tag{11}$$

If the right side of Eq. (10) becomes zero, then it is considered that the one mass system does not move in the absolute coordinate system. Damping force F_d might be applied so that the right side becomes zero.

$$m(\ddot{x} + \ddot{z}) + c(\dot{x} + \dot{z}) + k(x + z) = c\dot{z} + kz - F_d = 0 \tag{12}$$

$$F_d = c\dot{z} + kz \tag{13}$$

The restoring force F_d, and optimal control are combined with feedback control. The purpose of feedback control is to incorporate the effects of ground motion observation errors and disturbances.

3.3 Energy function control [5]

The objective is to control vibration during small earthquakes and large base isolation displacement during a large earthquake by outputting a small hysteresis loop during a small earthquake and a large hysteresis loop during a large earthquake using an MR damper. Using Eq. (14) as an evaluation function, Eq. (15) is used as the damper force.

$$f_{(t)} = \frac{1}{2}m\dot{x}^2 + \frac{1}{2}kx^2 \tag{14}$$

$$F_{MR} = \lambda\sqrt{f_{(t)}} \tag{15}$$

m, mass; *k*, stiffness; *x*, relative displacement of MR damper (m); λ, control coefficient

4. Experiment result

4.1 Comparison of verification methods

The earthquake waves used for the experiment were the El Centro NS wave (1940) (El Centro), ground motion observed at JR Takatori Station during the Southern Hyogo Earthquake (1995) (Takatori), and ground motion of the N–S direction observed at the Sylmar County Hospital parking lot during the Northridge Earthquake (1994) (Sylmar). The input wave was changed to an experimental magnification.

The control rules used were “LQR1” for state feedback optimal control, “LQR2” for optimal control considering the effects of seismic waves, “LQR3” for state feedback optimal control considering restoration force, “EF1” for state feedback energy function control, and “EF2” for state feedback energy function control considering the restoring force. Each weighting factor was found from a parameter study. The E-Defense experiment results were compared with those obtained using RTHS and the analysis. Figs. 6–8 present time history waveforms of the absolute acceleration of the specimen, the base-isolation layer displacement, the damper force, the displacement-damper force hysteresis, and the velocity-damper force hysteresis. Table 3 shows the correlation coefficients. The time history waveforms are very similar: the correlation coefficient shows a high value. However, some cases exist in which the correlation coefficient of the analysis is better than that of RTHS for E-Defense. Differences are apparent in results obtained from E-Defense, the analysis, and RTHS in terms of the displacement damper force hysteresis and the velocity-damper force hysteresis. In a region where the speed is high, the slope of the velocity-damper force hysteresis in the E-Defense experiment is small. It could not be confirmed whether this fact is attributable to modeling or to the fluid inside the damper.

4.2 Comparison of control methods

Study of control using RHTS reveals the points below. Fig. 11 presents the displacement-damper force hysteresis, and the velocity-damper force hysteresis. Figs. 12, 14, and 16 show the maximum base-isolation layer displacement on the x-axis and the maximum absolute acceleration on the y-axis. Figures 13, 15, and 17 present the RMS value of the base-isolation layer on the x-axis and the RMS value of absolute acceleration on the y-axis. Generally, it can be said that control improves as one approaches the origin.

Apparently, LQR1 can reduce the base-isolation layer displacement compared to 0A; the absolute acceleration does not increase to any marked degree. Furthermore, better results are obtained for both the base-isolation layer displacement and the absolute acceleration compared to those obtained for viscous damping control. However, for seismic waves such as Takatori and Sylmar, which include large short-period pulse components, further control is required. For seismic waves such as El Centro, the base-isolation layer displacement can be reduced considerably. Also, the absolute acceleration, which is regarded as an effective control, is not increased. Results show that LQR2 and LQR3 are close to the origin both for the maximum and RMS values for these ground motions. LQR2 has made it possible to reduce the absolute acceleration further. Also, LQR3 has made it possible to reduce the base-isolation layer displacement without increasing the absolute acceleration compared to LQR1.

Good control effects were expected from consideration of the restoring force in the energy function control. However, the experiment was apparently performed with the wrong setting of the weighting factor. The displacement between layers can be reduced compared to the viscous damping control, and the absolute acceleration was equivalent to 20% in Takatori and Sylmar.

4.3 Time delay of a real-time hybrid simulation

Fig. 18 presents part of the displacement of the shaking table at the time of El Centro of RTHS. Results show that the response displacement has a time delay of about 0.03 s with respect to the target displacement. Figures 19 show the frequency response of the response displacement to the target displacement. Results showed that the phase decreased by approximately 5–10 Hz, but it depends on the seismic waves and the measurement time. However, the time delay effect is apparently small because this study examines the base isolation for the structure.

Table 3 – Correlation coefficients

		Displacement	Absolute Acceleration	Damper Force
El Centro	E-defense • RTHS	0.9916	0.9445	0.9492
	E-defense • Simulation	0.9909	0.9476	0.9875
	RTHS • Simulation	0.9819	0.9850	0.9663
Takatori	E-defense • RTHS	0.9929	0.9459	0.9344
	E-defense • Simulation	0.9779	0.9396	0.9579
	RTHS • Simulation	0.9913	0.9972	0.9267
Sylmar	E-defense • RTHS	0.9897	0.9054	0.8528
	E-defense • Simulation	0.9930	0.9124	0.9412
	RTHS • Simulation	0.9875	0.9962	0.8666

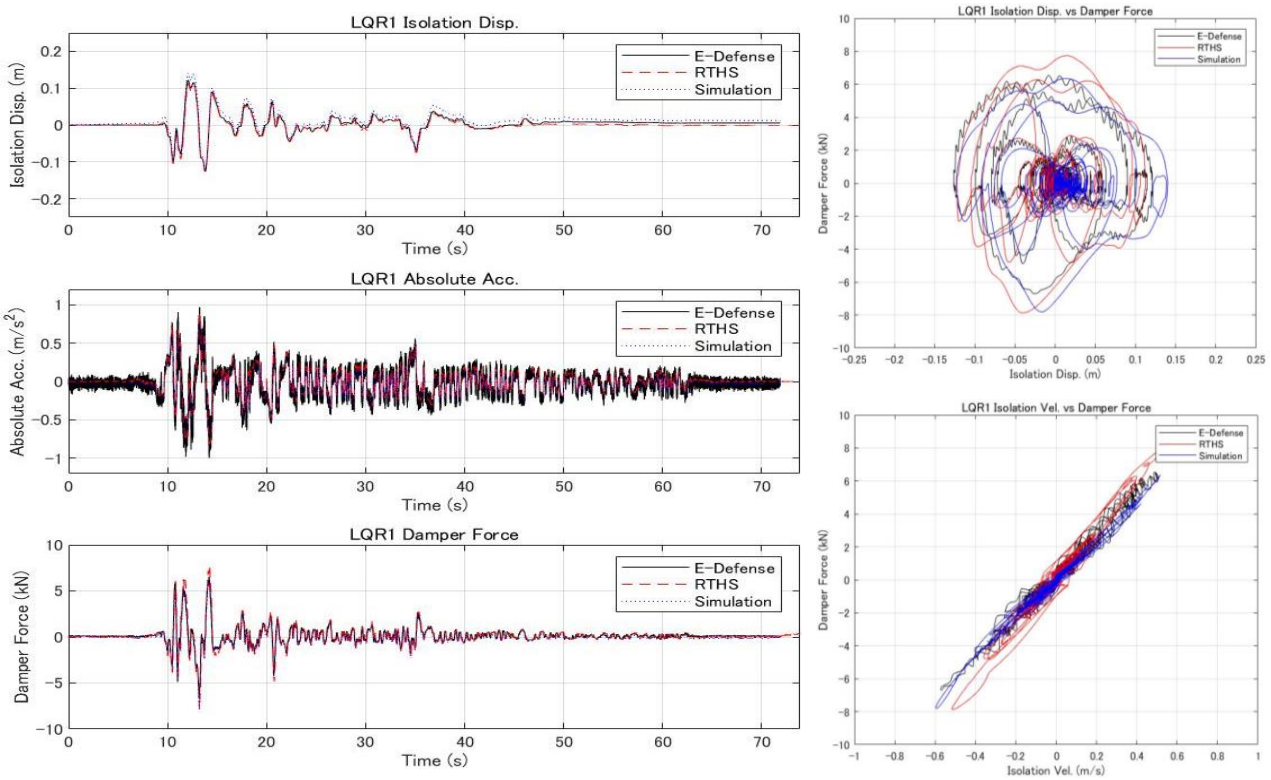

Fig. 8 – Verification methods (El Centro)

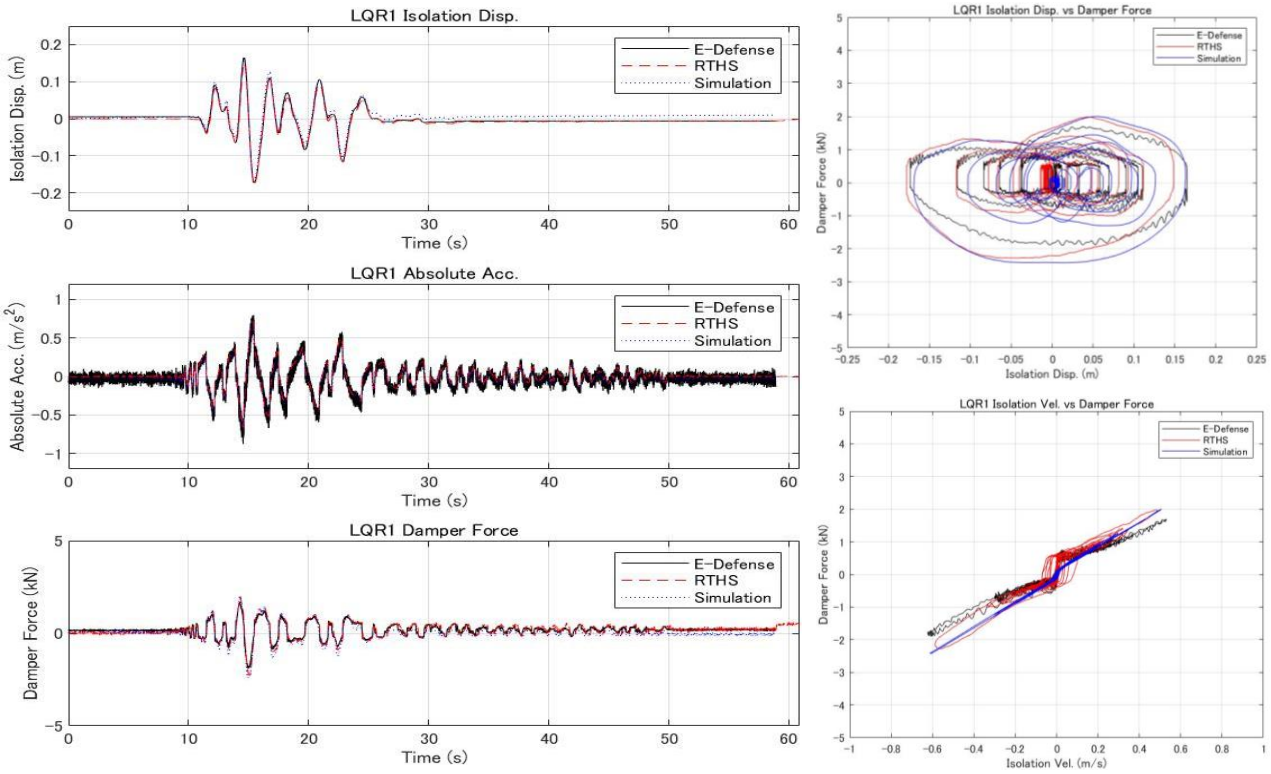

Fig. 9 – Verification methods (Takatori)

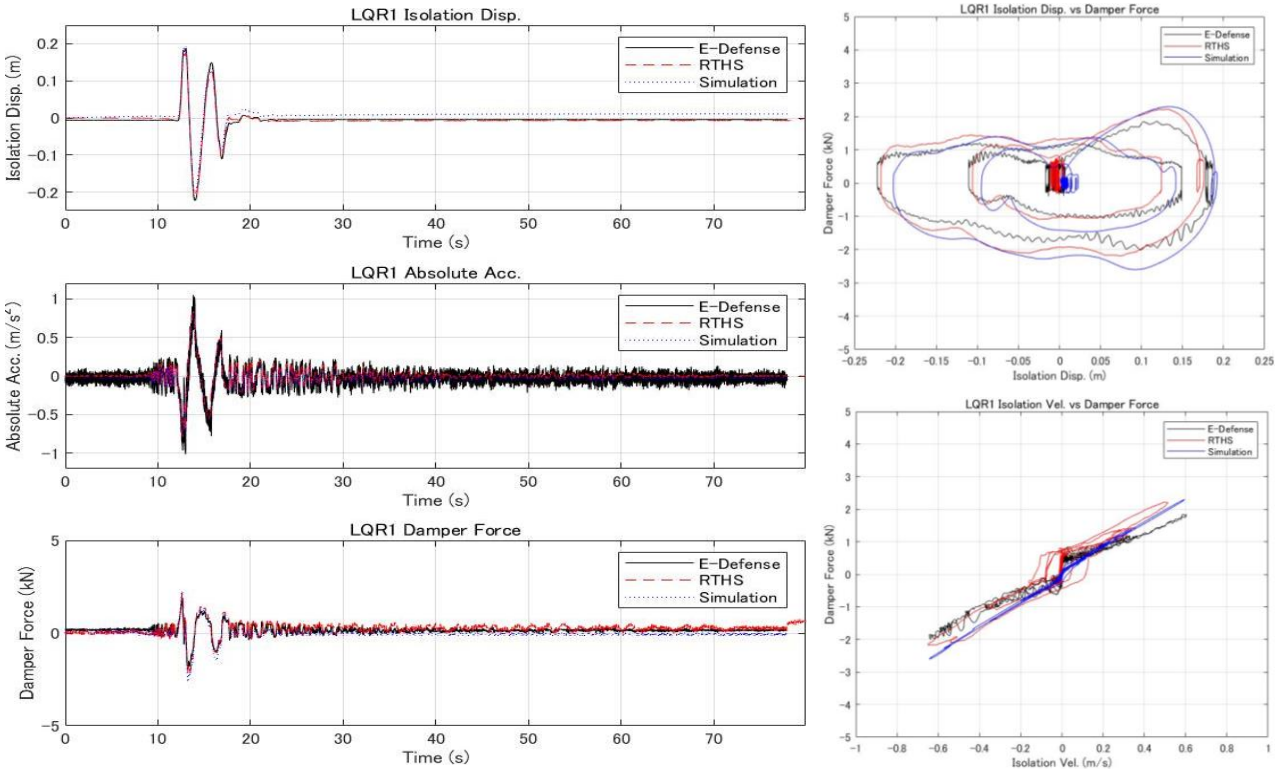

Fig. 10 – Verification methods (Sylmar)

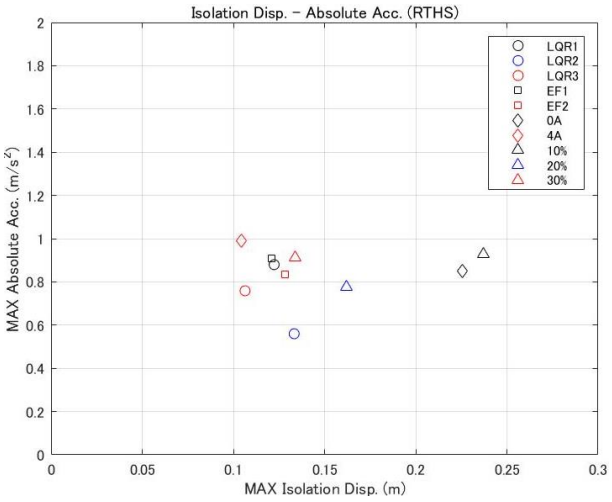

Fig. 11 – Max. comparison (El Centro)

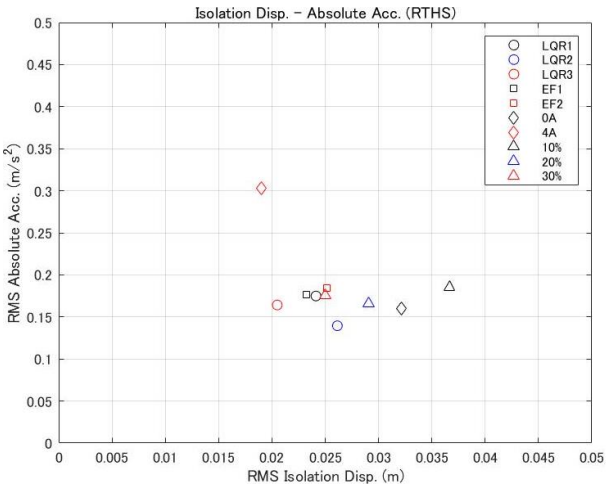

Fig. 12 – RMS value comparison (El Centro)

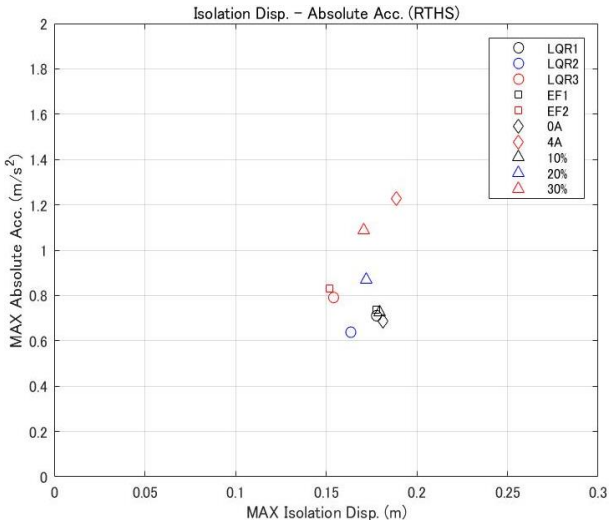

Fig. 13 – Max. comparison (Takatori)

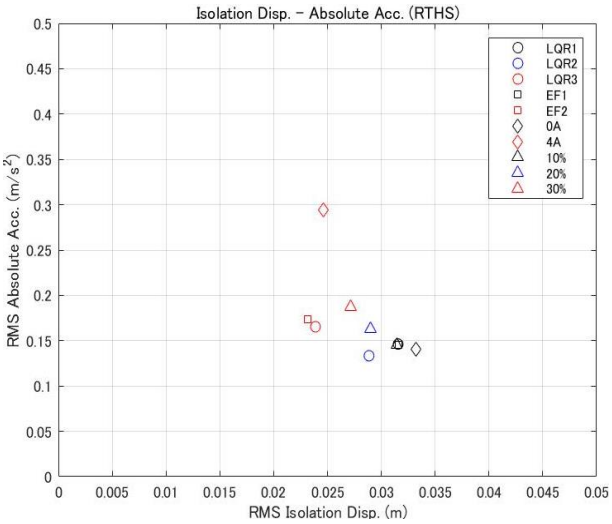

Fig. 14 – RMS comparison (Takatori)

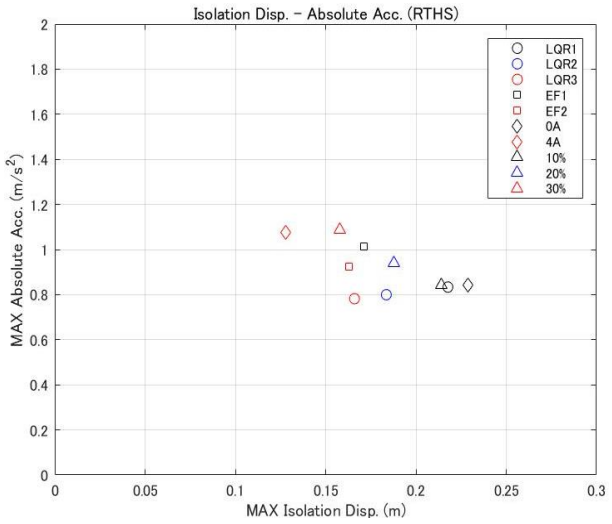

Fig. 15 – Max. comparison (Sylmar)

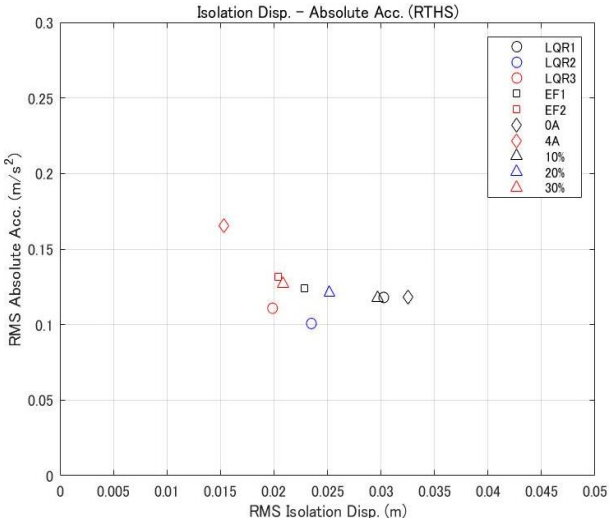

Fig. 16 – RMS comparison (Sylmar)

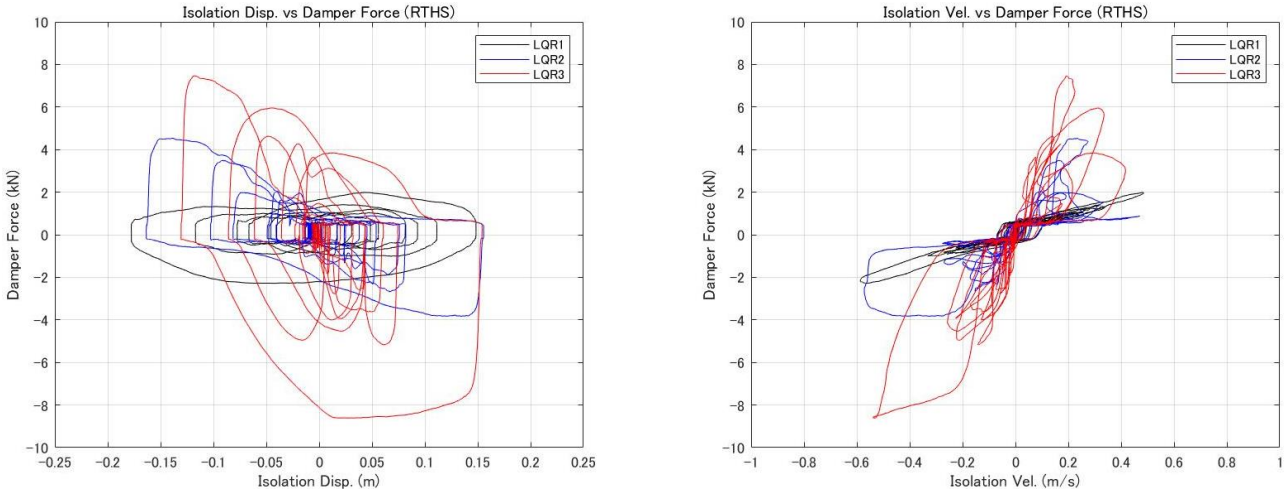

Fig. 17 – Comparison of LQR (Takatori)

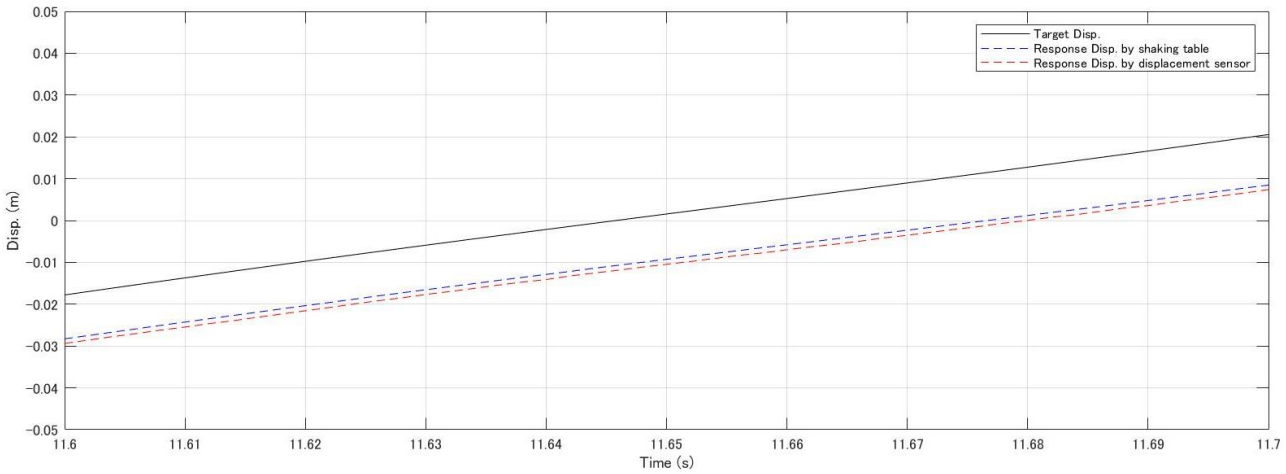

Fig. 18 – Time delay of RTHS (El Centro)

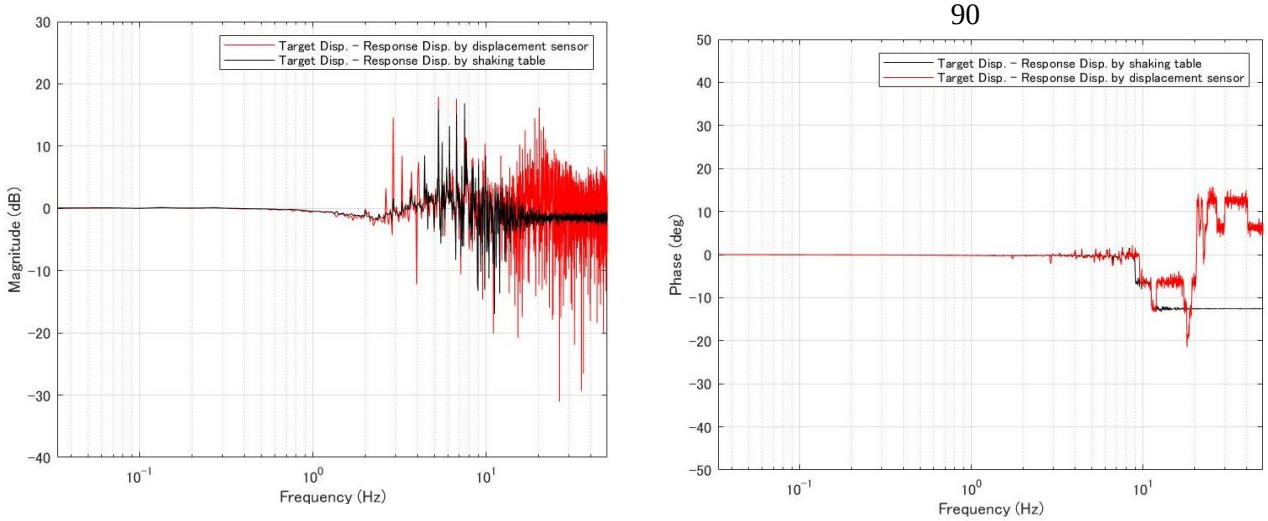

Fig. 19 – The frequency response of the response displacement to the target displacement (El Centro)

5. Conclusion

To confirm the effectiveness of the semi-active control effect, we conducted shaking table experiments at E-Defense and conducted an RTHS at Kobe University.

The effectiveness of RTHS was confirmed by comparing RTHS obtained from E-Defense experiments and from computer analysis. Both the time history waveform and the correlation coefficient showed good correspondence. However, some cases exist in which the correlation coefficient of the analysis is better than that of RTHS for E-Defense. It was not possible to confirm whether the cause was the influence of modeling or the influence of the fluid inside the damper where the damper force did not derive from the ideal value.

For RTHS, the effectiveness of semi-active control was confirmed by comparing semi-active control with passive control. The control effect was confirmed as obtainable using optimal control rather than the passive control. Additionally, further control effects were confirmed as obtainable by considering seismic wave effects. However, the control effect differs depending on the seismic waves and building specifications.

Acknowledgments

This work was supported by JSPS Grant No. R2904 in the Program for Fostering Globally Talented Researchers and the research unit of Multidisciplinary Integration for Resilience and Innovation (MIRAI) in Kobe University.

References

[1] Hakuno M, Shidawara M, Hara T (1969): Dynamic destructive test of a cantilever beam, controlled by an analog-computer, *Proc. Jap. Soc. Civil. Eng*., (in Japanese), 171, pp. 1-9.

[2] Keiju I, Ito M, Fujitani H, Iba S (2019): Shaking Table Test and Real Time Hybrid Test in Semi-Active Controlled Base Isolation System Part 3 Consideration of Modeling for MR damper Considering Frequency Response, *Summaries of Technical Papers of Annual Meeting Architectural Institute of Japan*, (in Japanese), 21041, pp. 81-82.

[3] Yoshida K, Fujio T (2001): Bilinear Optimal Control Theory and its Application to Semi-Active Vibration Isolation Control, *Transactions of the Japan Society of Mechanical Engineers. C*, (in Japanese), 656, pp. 96-102.

[4] Yoshida O, Kageyama M, Sano T, Endo F, Watanabe T, Katsumata H (2010): Super Active Base Isolation System "Laputa 2D", *Report of Obayashi Corporation Technical Research Institute*, (in Japanese), 74, pp. 1-8.

[5] Shiozaki Y, Hiwatashi T, Fujitani H, Soda S (2003): Simple Semi-Active Control for Base-Isolation Building by MR Damper, *Journal of Structural and Construction Engineering*, (in Japanese), 570, pp. 37-43.

